Journal of Power Sources 297 (2015) 188–194

Contents lists available at ScienceDirect

Journal of Power Sources

journal homepage: www.elsevier.com/locate/jpowsour

High-rate lithium–sulfur batteries enabled by hierarchical porous carbons synthesized via ice templation

Ritu Sahore [a], Luis P. Estevez [a], Anirudh Ramanujapuram [a], Francis J. DiSalvo [b], Emmanuel P. Giannelis [a, *]

[a] Department of Materials Science and Engineering, Cornell University, Ithaca, NY 14853, USA
[b] Department of Chemistry and Chemical Biology, Cornell University, Ithaca, NY 14853, USA

HIGHLIGHTS

- Porous carbons synthesized via ice templation were tested as sulfur hosts.
- Extremely high surface area and pore volume led to good high C-rate performance.
- Studied capacity decay in the presence of $LiNO_3$ electrolyte additive.
- Demonstrated independence of pore size and capacity decay in the above study.

GRAPHICAL ABSTRACT

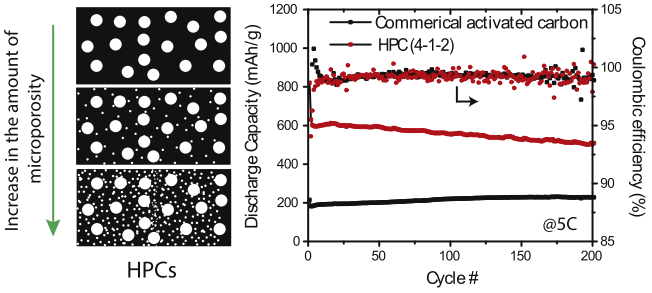

ARTICLE INFO

Article history:
Received 25 March 2015
Received in revised form
5 July 2015
Accepted 22 July 2015
Available online xxx

Keywords:
Hierarchical porous carbons
Lithium–sulfur batteries
Cyclic performance
Porosity dependence
Lithium nitrate

ABSTRACT

We report the performance of a series of hierarchical porous carbons (HPCs) with extremely high surface areas of up to 2340 $m^2\ g^{-1}$ with total pore volume of up to 3.8 $cm^3\ g^{-1}$ as supports for sulfur for Li–S batteries. The hierarchical structure of the carbon originating from interconnected large mesopores (10–50 nm), small mesopores (2–10 nm) and micropores (<2 nm) makes the total available surface area highly accessible, resulting in excellent electrode kinetics. At high C-rates of 2 C and 5 C, large specific capacities of 647 mA h g^{-1} and 503 mA h g^{-1}, respectively, were obtained after 200 cycles. In addition, we also systematically show that the cyclic stability is independent of the size of the pores sulfur is initially confined in, when $LiNO_3$ is used as the electrolyte additive, indicating that capacity fade due to polysulfide shuttle is effectively eliminated and that it is not related to pore size anymore.

1. Introduction

Several issues with the present cathode materials involved in the current rechargeable lithium-ion battery technology have led to a vast new research area in search of new rechargeable battery systems which incorporate inexpensive, light weight active materials and most importantly have much higher theoretical specific capacities and energy densities [1]. Lithium-sulfur is one such system that has a theoretical specific capacity of 1672 mA h g^{-1} and theoretical specific energy of 2567 W h kg^{-1}, which are almost an order of magnitude higher than the current lithium-ion batteries, due to the light weight of sulfur and a high charge storage of $2e^-$ per S atom [2,3]. Sulfur is also non-toxic, highly abundant and cheap. Yet, there are many problems associated with this system, primarily, lower than theoretical specific

* Corresponding author.
E-mail address: epg2@cornell.edu (E.P. Giannelis).

http://dx.doi.org/10.1016/j.jpowsour.2015.07.068
0378-7753/

capacities and poor cycle life. Both of these problems have been linked with the insulating nature of sulfur and with the high solubility of the electrochemical reaction intermediates called "polysulfides" in the electrolyte. The former makes sulfur that is not very close to the carbon surface (more than a few tens of nanometers) essentially electrochemically inactive and the later causes the loss of active material as the polysulfides dissolve and diffuse towards the lithium metal anode and react with the Li to irreversibly form insoluble and electrically insulating Li_2S_2 or Li_2S [4–8].

Among the various candidate materials, porous carbons have received great attention since they provide a high surface area, electrically-conductive framework on which insulating sulfur can be made electrochemically active when properly dispersed [9–17]. Besides, the sorption effect of polysulfides on the carbon surface is known to impede their diffusion into the electrolyte [9]. But the kind of porosity in these carbons is very crucial in their overall battery performance including specific capacity values, cycle life, and rate capability. Mesopores (2–50 nm) have been shown to be the most effective in getting close to theoretical specific capacities at high rates due to fast transport of Li^+ ions in and out of the electrode. For example, a bimodal mesoporous (3.1 nm and 6 nm) carbon support in the form of 300 nm diameter spherical particles was shown to give high specific capacity of up to 1200 mA h g^{-1} at a high C-rate of 1 C [18]. Micropores (<2 nm), on the other hand, due to their smaller size are the most effective in trapping polysulfides [19–23]. Completely microporous carbons have been shown to have excellent long cycle life even in the reportedly polysulfide-incompatible carbonate-based electrolytes [24]. But limiting the size of the pores leads to poor Li^+ ion kinetics and the specific capacities drop significantly at high C-rates. Hence, to achieve higher specific capacities at fast charge/discharge rates, a framework which is open, but still has large surface area seems the most desirable. In fact, nanocarbons like CNTs and stacked graphene, which generally have low surface area, showed greatly improved performance with cycling at rates up to 10 C upon incorporating mesopores or micro-/meso-hierarchical porosity [25].

Here, we report the high C-rate performance of a series of hierarchical porous carbons (HPCs) with extremely large surface areas up to 2340 m^2 g^{-1} and pore volumes up to 3.8 cm^3 g^{-1}, which is among the highest for similar systems reported previously for this application [22,23,26–29]. The carbons are prepared via a two-step process of hard templation followed by physical activation for different time durations. The detailed synthesis of similar carbons was reported earlier by our group [30]. Since the highly open nature of the carbon framework facilitates the Li^+ ion diffusion in and out of the electrode, it also makes the out diffusion of the polysulfides easier. To prevent active material loss via diffusion and its reaction with lithium anode, $LiNO_3$ salt was used as an electrolyte additive, which has been shown to make a stable and Li^+ ion conducting solid–electrolyte interface (SEI) on the lithium metal surface inhibiting the shuttle mechanism that limits the cycle life [31–36]. We systematically show that in the presence of $LiNO_3$ additive, cyclic stability while improved is rather independent of the size of the pores where the sulfur is initially confined in, indicating effective suppression of capacity loss due to polysulfide shuttle or the presence of other capacity loss mechanisms to cause a gradual decay in capacity over cycling. Lastly, the performance of the HPCs is compared and contrasted with cathodes prepared using a commercially available microporous carbon. We show that the HPCs consistently outperform the commercially available carbon signifying that the intricate network of hierarchical porosity is critical for good performance.

When tested as supports for sulfur at a ~50 wt. % S loading using ether based DOL/DME electrolyte with $LiNO_3$ additive, these HPCs showed excellent high rate performance with exceptionally high capacities of up to 647 mA h g^{-1} and 503 mA h g^{-1} (per gram of sulfur) at 2C, and 5 C rates respectively after 200 cycles, with ~99% coulombic efficiencies. In contrast, a commercial microporous carbon gave a much lower initial capacity of 345 mA h g^{-1} @1 C under similar sulfur loading indicating much slower Li^+ transport kinetics in the cathode. Moreover, @1 C similar capacity retention values of 80–85% from the 10th to 100th cycle were observed for all the carbons despite their different textural characteristics confirming our result that cyclic stability is independent of the size of pores sulfur is initially confined in.

2. Experimental section

2.1. Preparation of mesoporous and activated mesoporous carbons

HPCs were synthesized using a slight modification of our previously reported procedure [30]. The nomenclature of HPCs is in the following format: A-x-y, where A is the size of the colloidal silica template used (as provided by the supplier), x is the weight ratio of colloidal silica to sucrose, and y is the time of CO_2 activation. To synthesize 4-1-0 carbon, 6 g sucrose was dissolved in 40 g of a 15 wt. % colloidal silica suspension in so as to achieve 1:1 weight ratio of sucrose to silica content. The solution was frozen by plunging the container in liquid nitrogen and then immediately transferred to a freeze dryer to sublime away the ice. The sublimation time was approximately 48 h to ensure complete removal of the ice. The melting point of the freeze dried composite remains above room temperature under the vacuum conditions of 0.014 mBar inside the freeze drier jar, which prevents its melting during dying. After that, the sucrose-silica composite was carbonized in an inert atmosphere of argon gas while heating with a ramp rate of 180 C h^{-1} to1000 °C for 3 h. To remove the silica, the carbonized material was etched using a stirred 3 M NaOH solution at 80 °C for 24 h. Finally, the sample was washed with deionized water until a neutral pH solution is obtained and then kept in a vacuum oven at 80 °C for at least 24 h for drying. CO_2 activation of the carbon was carried out in a tube furnace at 950 °C by flowing CO_2 gas over the carbon at 50 cm^3 min^{-1} for various times from 0 to 2 h. The sample was never exposed to air during the activation cycle. 4-0.5-0 carbon was synthesized using the same procedure as above, except the silica to sucrose weight ratio was changed to 0.5.

2.2. Preparation of carbon–sulfur composites

Carbon-sulfur composites were prepared via melt infusion. Typically, carbon and sulfur powders were taken in a 1:1 weight ratio and mixed well in a mortar and pestle to ensure uniform dispersion on the micron scale of sulfur particles in the carbon. The mixture was then transferred to a stainless steel Parr reactor and placed in an oven heated at 160 °C for 18 h to obtain the C–S composites.

Structural characterization: Nitrogen adsorption and desorption isotherms were obtained at 77 K using a Micromeritics ASAP2020 instrument. Specific surface areas and pore volumes were calculated using the Brunauer–Emmett–Teller (BET) and Barrett–Joyner–Halenda (BJH) models, respectively, applied on the adsorption branches of the adsorption–desorption isotherms. TG/DTA analysis was performed using EXSTAR TG/DTA6200, where the samples were heated at a rate of 10 °C/min from room temperature to 500°. XRD traces were obtained using a Scintag Theta–Theta X-Ray Diffractometer with Cu Kα radiation.

2.3. Electrochemical testing

The cathode was prepared by making a slurry of the carbon-

sulfur composite, SuperP carbon black, and polyvinyledene fluoride (PVDF) binder in a weight ratio of 80:12:8, using N-methyl-2-pyrrolidone as the solvent. The slurry was then cast onto an aluminum foil using a doctor blade to make ~20 micron thick films followed by drying at 70 °C in an oven for 15 h. Typical sulfur loading per electrode was 0.35–0.50 mg cm^{-2}. Hence, a tap-density of ~0.18–0.25 g cm^{-3} was obtained for a typical electrode. Lithium metal (Alfa Aesar) was used as the anode. A microporous polypropylene Celgard membrane was used as the separator. 1 M Lithium Bis (Trifluoromethanesulfonyl) Imide (LiTFSi) (Sigma Aldrich) and 1wt% lithium nitrate ($LiNO_3$) dissolved in a mixture of 1, 3-Dioxolane (DOL) and Dimethoxyethane (DME) (1:1 by volume) was used as the electrolyte. CR2032 type coin cells were assembled in a glove box under inert argon atmosphere. Galvanostatic charge and discharge tests were carried out using a MACCOR battery tester in the voltage range of 1.7–2.8 V (vs Li^+/Li). All specific capacities were calculated per gram of sulfur unless otherwise mentioned (so the mass of carbon, PVDF and Al is not included.) C-rates are used to describe charge/discharge rates, where, 1C = complete discharge/charge in 1 h (for sulfur, the theoretical value is 1672 mA h g^{-1} for complete conversion of S to Li_2S).

3. Results and discussion

3.1. Morphology of HPCs

HPCs with very high surface areas and pore volumes of up to 2340 m^2 g^{-1} and 3.8 cm^3 g^{-1} were synthesized via physical activation of mesoporous carbons using CO_2 gas for different times. The mesoporous carbons were prepared via ice templating a suspension of colloidal silica (hard template) with sucrose (carbon precursor) in liquid nitrogen at 77 K, followed by freeze drying, carbonization at 1000 °C, and etching to remove the silica. The above process is key to obtaining mesopores with very tight size control. These pores correspond well with the colloidal silica size as ice templation locks the structure in place and prevents the aggregation of silica particles, giving rise to high surface area and pore volume. Hence, the carbon framework before activation is already very open due to these interconnected mesopores. Fig. 1a, b shows a foam-like morphology as seen under TEM. It is noteworthy to mention here that the inexpensive precursors and uncomplicated synthesis steps make the synthesis easily scalable.

Table 1 lists the textural characteristics of all the carbons that were synthesized and measured using nitrogen adsorption at 77 K. To remind, we use the following format for naming HPCs: A-x-y, where A is the size of the colloidal silica template used (as provided by the supplier), x is the weight ratio of colloidal silica to sucrose, and y is the time of CO_2 activation. Zero hours of activation represents a non-activated, completely mesoporous carbon. As can be seen from the Table, longer activation times lead to higher surface areas and pore volumes. This is attributed to introduction of micropores and small mesopores along with broadening of the existing mesopores. Micropore volume (obtained by the t-Plot analysis method), increased from 0.06 cm^3/g for unactivated carbon to 0.20 cm^3 g^{-1} after 2 h of activation. A breakdown of cumulative pore volume into three different mesopore sets as they evolve upon activation is also listed in the Table. The small amount of microporosity even in the unactivated carbon was present probably due to the evaporation of volatiles formed during carbonization of sucrose.

The nature of overall porosity of the HPCs and its evolution upon activation can be seen more clearly from the adsorption/desorption isotherms and BJH adsorption pore size distribution plots (Fig. 1c, d). The original mesoporous carbon shows two distinct capillary condensation steps in the isotherm, the first starting at p/p0 ≈ 0.6 and the second at p/p0 ≈ 0.8, corresponding to two different sets of mesopores. The former occurs due to uniform mesopores of average size of 7 nm corresponding to the sharp peak in the pore-size distribution plot. These pores correlate well with the size of colloidal silica template used. The second condensation step is due to mesopores of size from 10 to 30 nm and corresponds to the broad shoulder to the right in the pore-size distribution plot. These larger pores come from slight aggregation of colloidal silica, which occurs when there is not enough sucrose to wrap around all the particles, which happens to be the case for this particular silica to sucrose weight ratio of 1:1. This broad shoulder as well as the second

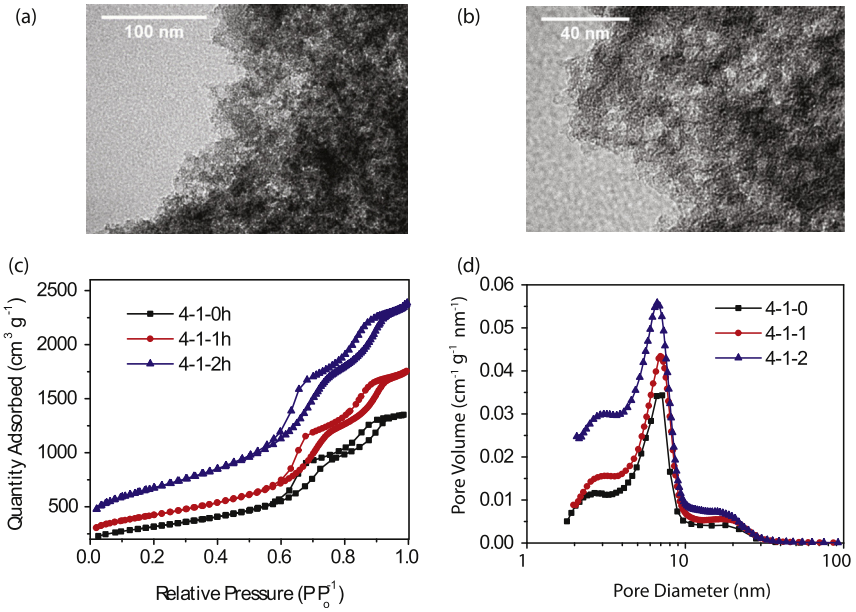

Fig. 1. (a, b) TEM images of 4-1-0 carbon showing foam-like morphology with interconnected disordered mesopores; (c) Adsorption–desorption isotherms, and (d) BJH poresize distribution plots of activated carbons, obtained via nitrogen sorption measurement at 77 K.

Table 1
Porosity characteristics of all HPCs obtained via nitrogen adsorption at 77 K. A breakdown of total pore volume into different mesopore regimes is listed. Increased surface area and pore volume is observed with longer activation times. See text for explanation of symbols and labeling scheme.

Carbon	S_{BET} ($m^2\ g^{-1}$)	V_{meso} ($cm^3\ g^{-1}$)	V_{micro} ($cm^3\ g^{-1}$)	V_{2-4nm} ($cm^3\ g^{-1}$)	V_{4-10nm} ($cm^3\ g^{-1}$)	$V_{>10nm}$ ($cm^3\ g^{-1}$)
4-1-0	1110	2.12	0.06	0.24	1.12	0.70
4-1-1	1473	2.0.77	0.12	0.31	1.50	0.96
4-1-2	2339	3.81	0.20	0.56	2.07	1.17

condensation in the isotherm were absent when the ratio was decreased to 0.7 (SI Figure S1) indicating tight control of this region of mesopores. There is a small shoulder to the left of the peak as well in the mesopore range of 2–4 nm. This may be explained by the incomplete filling of inter-particle spaces by sucrose during ice templation, which show up as pores after carbonization and etching. Upon activation, both the isotherms and pore-size distribution plots indicate that all pores become larger and the distribution of pore diameters broaden somewhat consistent with the increase in surface area and pore volume due to the introduction of new micropores, small mesopores and broadening of the existing mesopores. TEM images of the activated carbons also confirm that the original mesoporous framework does not collapse upon activation (SI Figure S2). Care must be taken to not activate for longer periods, as it eventually leads to collapse of the mesoporous network causing lowering of both surface area and pore volume.

To measure the degree of graphitization of HPCs, XRD and Raman Spectroscopy testing were performed (SI Figure S3), both of which show that the carbons are partially graphitic.

3.2. Characterization of HPCs–S composites

To test the performance of HPCs as supports, composites with sulfur from various carbons were synthesized. Sulfur was introduced into the pores of these carbons via the melt-infusion method, where carbon and sulfur powders were heated together at 160 °C so as to liquefy the sulfur in and allow it to infuse into the pores via capillary forces. The vapor pressure of sulfur at this temperature is 0.3 torr, so infiltration may include transport through the vapor phase as well. The sulfur content in the C–S composites made from 4-1-0, 4-1-1, 4-1-2 carbons was determined using thermogravimetric analysis (TGA) to be 50.0 wt. %, 47.5 wt. %, and 47.4 wt. %, respectively.

To confirm that melt infusion successfully infused the sulfur into the pores, TGDTA, XRD, and SEM-EDX were used (Fig. 2). Pore size distribution analysis of carbon-sulfur composites was also performed to further confirm this (SI Figure S4). As can be seen from Fig. 2a, a shift in the TG curves to higher temperatures was seen for activated carbons. This shift can be seen more clearly in the DTG curves (Fig. 2b) where the peak corresponding to highest rate of sublimation of sulfur, shifts and broadens towards higher temperatures with longer activation times. This effect can be attributed to the presence of sulfur in the micro- and small mesopores and the stronger confinement of sulfur in these smaller pores [23]. To confirm that indeed the sulfur is confined more strongly in micropores, a sulfur composite was made with an almost completely microporous carbon (commercially available from MTI Corp.) having a micropore volume of 0.46 $cm^3\ g^{-1}$ and total pore volume of 0.51 $cm^3\ g^{-1}$. Nitrogen adsorption/desorption isotherms as well as pore-size distribution plots are provided in the Supporting Information (SI Figure S5). Since, based on the density of liquid sulfur at melt-infusion temperature (1.76 g cm^{-3}), a minimum pore volume of 0.55 $cm^3\ g^{-1}$ is required to accommodate all sulfur at 49.2 wt.% S loading, most of the sulfur should get accommodated in the micropores of this carbon. Expectedly, the TG/DTA results of this carbon's composite showed the most delayed sulfur sublimation and the DTG peak appeared after 400 °C, which is more than 100 °C higher than the other carbons. Therefore, from the DTG plots it was inferred that sulfur's location varies in all three carbons (as can be visualized from the Schematic in Fig. 2e), filling up the micropores first due to their smallest size, followed by small and then large mesopores.

In the 4-1-0 carbon, the pore volume from micropores is negligible, hence most of the sulfur is expected to be uniformly dispersed in the mesopores. Whereas in 4-1-2 carbon, the pore volume below 2 nm is 0.20 $cm^3\ g^{-1}$, which is 39% of the theoretical pore volume of 0.51 $cm^3\ g^{-1}$ required to fill up with liquid sulfur @47.5wt% S loading, which implies that the micropores contain 39% of the total S. Hence, the sulfur is in a much more dispersed state in the 4-1-2-S composite with an expectedly much thinner sulfur coating on the mesopore walls as compared to the unactivated carbon 4-1-0-S composite.

The good dispersion of the sulfur in the porous network was further confirmed by X-ray diffraction. No crystalline peaks of sulfur were observed for all three HPC-S composites, indicating that sulfur was well dispersed in the meso/micropores (Fig. 2c). Due to the small particle size of sulfur in the dispersed state, only an amorphous signal in the XRD is observed [9]. SEM-EDX elemental mapping on a composite particle also confirmed the uniform distribution of sulfur in the carbon (Fig. 2d).

3.3. Electrochemical performance

To test the performance of HPCs as sulfur supports and to understand how morphology affects the battery performance, coin cells were assembled using electrodes made out of C–S composites of the all three carbons and galvanostatically cycled with lithium metal as the anode in a voltage range of 1.7–2.8 V. DOL/DME electrolyte with 1 wt. % $LiNO_3$ was used as the electrolyte. Coin cells were cycled at different C-rates ranging from 0.1 C up to 5 C. Fig. 3a shows the cyclic performance of the composites from 4-1-0, 4-1-1 and 4-1-2 at a 1 C rate. Typically battery capacity increases with longer activation process times. The initial capacity increased from 1101 mA h g^{-1} for the unactivated carbon to 1198 mA h g^{-1} and 1287 mA h g^{-1} for carbons activated for 1 h and 2 h respectively. After 100 cycles, the capacities were 555 mA h g^{-1}, 682 mA h g^{-1} and 747 mA h g^{-1}, respectively.

Since the composite from 4-1-2 carbon showed the highest capacity, all further high C-rate tests were performed on this carbon. Fig. 3b shows the galvanostatic charge–discharge profiles obtained in the 10th cycle at various C-rates. At 0.1 C, a capacity of 954 mA h g^{-1} was obtained which only dropped to 864 mA h g^{-1}, 789 mA h g^{-1}, and 601 mA h g^{-1} @ 1 C, 2 C and 5 C rates, respectively. Moreover, well defined plateaus with relatively small electrode polarization were observed going from 0.1 C to 5 C. The second discharge plateau was still above 2 V at 2 C and decreased to only 1.95 V at 5 C. These results indicate excellent overall kinetics due to fast lithium ion transfer in and out of the electrode. With long-term cycling at 2 C and 5 C, capacities of 647 mA h g^{-1} and 503 mA h g^{-1} were still obtained after 200 cycles while maintaining ~99% coulombic efficiencies (Fig. 3c).

To confirm that a hierarchical porous network is essential to

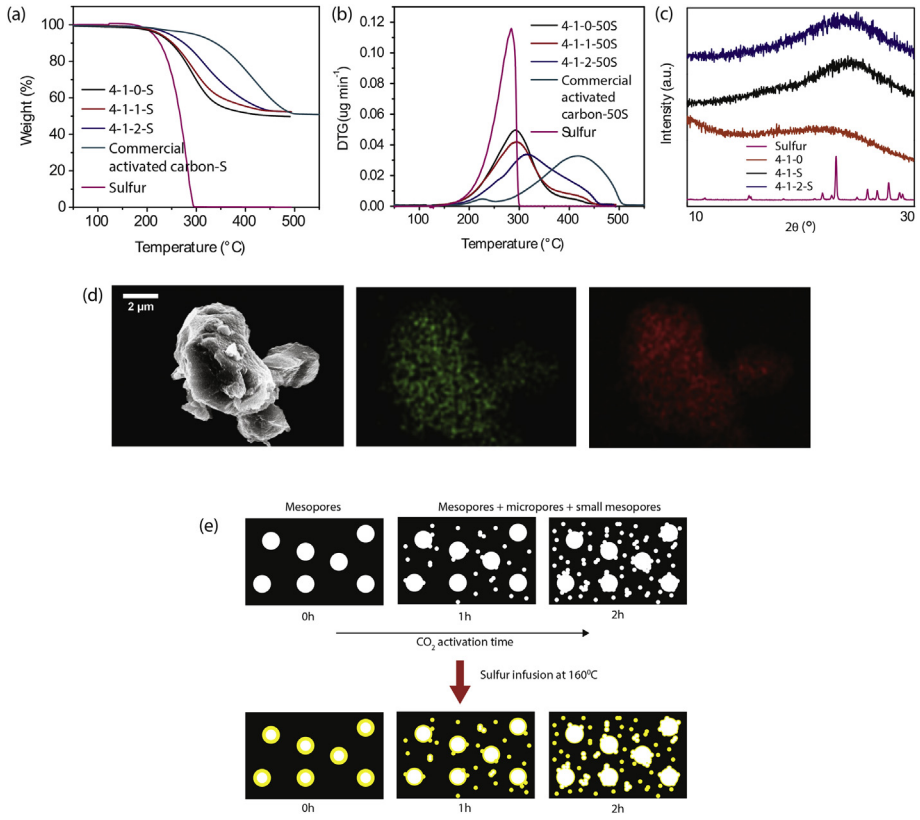

Fig. 2. Characterization of HPC-S composites: (a, b) TG and DTG profiles of sulfur composites made with 4-1, 4-1-1, 4-1-2, and commercial activated carbon. (c) XRD plots of pure sulfur, HPC 4-1 before and after sulfur infiltration at 159 °C. (d) SEM-EDX elemental mapping of S and C on an HPC-S nanocomposite particle. (e) A schematic of porosity evolution upon activation and sulfur dispersion in those carbons.

high specific capacities at fast charge/discharge rates, a commercially available microporous carbon was tested as a control sample. This carbon has a surface area of 1856 $m^2\ g^{-1}$ and pore volume of 0.51 $cm^3\ g^{-1}$ arising almost entirely from micropores. The electrical conductivity was similar to that of HPCs (SI Table S1) allowing performance comparisons to be made only in terms of morphology/texture for the different materials. When tested at similar sulfur loading of 49.2% S, the microporous only carbon showed a much lower initial capacity of 547 mA h g^{-1} at 1 C indicating much slower Li^+ transfer kinetics (Fig. 3d) (Cycling performance data @1 C available in SI Figure S6). At 2 C and 5 C, much lower initial capacities of 427 mA h g^{-1} and 215 mA h g^{-1} were obtained. The corresponding values after 200 cycles were 316 mA h g^{-1} and 229 mA h g^{-1} respectively (Fig. 3e). In addition the electrode polarization was much more pronounced (Fig. 3f).

A fast capacity drop over the first 10 cycles was observed for all HPCs, which could be explained by the reaction of polysulfides that form during discharge with the $LiNO_3$ salt present in the electrolyte to form a solid electrolyte interface (SEI) layer on the lithium metal surface [36]. This layer supposedly protects the polysulfides that form later during cycling from reacting at the lithium anode, which also explains a much smaller capacity drop over the next 90 cycles. Interestingly, capacity retention values over 10th to 100th cycle were virtually the same (79%, 80% and 82% for composites from 4-1-0, 4-1-1 and 4-1-2, respectively). Longer activated carbons are expected to have a much higher fraction of sulfur in the micropores and small mesopores, which have been shown to be better sequester for polysulfides. However, all three carbons show the same capacity fade regardless of where the S resides. This strongly suggests that the presence of a stable SEI on the lithium anode, which is effective in preventing polysulfide shuttle, masks any effect of carbon porosity on capacity fade due to the shuttling. Approximately 99% coulombic efficiencies were obtained for all the carbons again indicative of suppressed polysulfide shuttling.

To better understand these results, we compared two HPC-S composites, where the sulfur was present exclusively in either mesopores or micropores. For this study, we chose mesoporous carbon 4-0.5-0 as the starting carbon, since it was possible to achieve higher micropore volume in this carbon upon activation due to the thicker mesopore walls. A micropore volume of 0.29 $cm^3\ g^{-1}$ was obtained in 4-0.5-3. Based on the micropore volume and density of liquid sulfur a theoretical sulfur loading of 33 wt. % is possible. Therefore, a sulfur loading of 30 wt. % was chosen to ensure that all the sulfur was present in the micropores of the activated carbon 4-0.5-3. Fig. 4a shows schematically the difference in sulfur confinement in the two carbons. TGDTA confirms that the sulfur is indeed located in the micropores (SI Figure S7). Similar capacity fade from both composites was observed when cycled at 1 C rate with a capacity retention of ~80% from 10th–100th cycle (Fig. 4b). These results reconfirm our conclusion that in the presence of $LiNO_3$ additive, the capacity fade is independent of size of the pore where sulfur is confined in. A much higher capacity, however, was obtained from 4 to 0.5-3 carbon-sulfur composite due to its significantly higher surface area and pore volume (SI Table S2). This result is in agreement with previous studies that used $LiNO_3$ additive [37,38]. The capacity fade in all the composites could be explained by the detrimental effects associated with the formation of insoluble Li_2S_2 and Li_2S upon discharge as was demonstrated in several recent reports where cycling between S and the soluble Li_2S_4

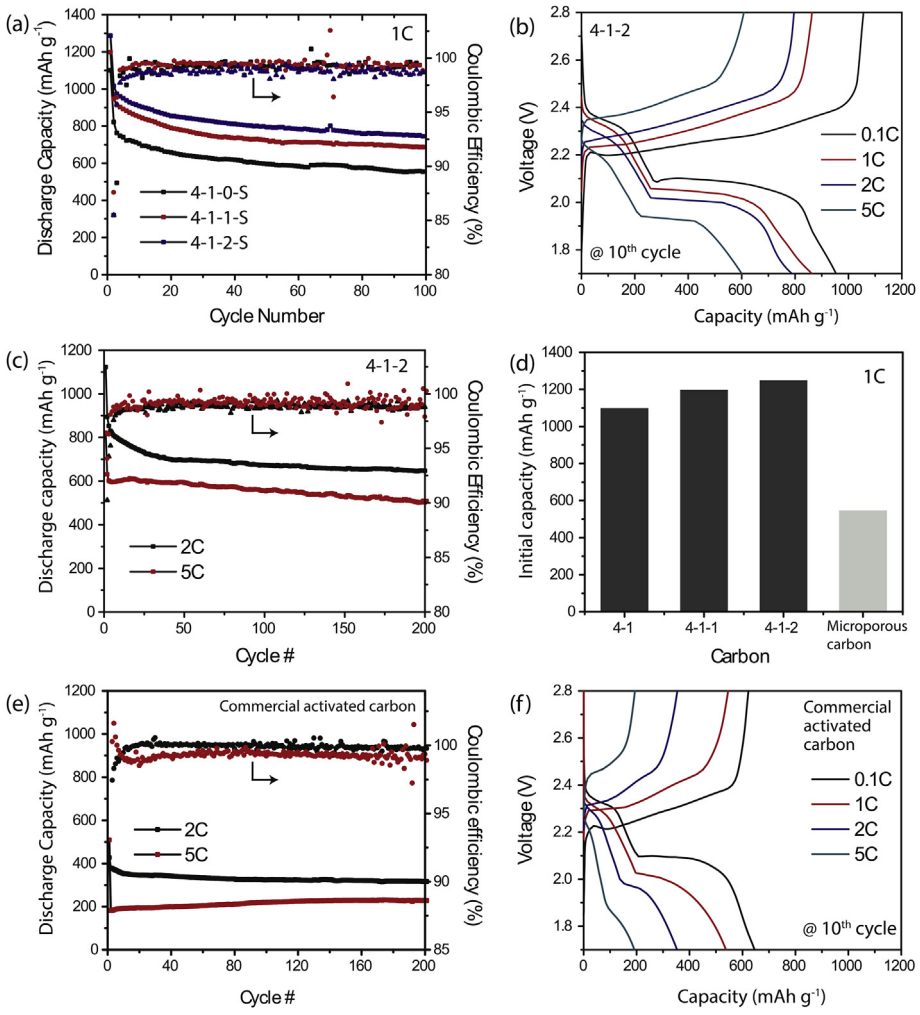

Fig. 3. Electrochemical performance of HPCs–S nanocomposites: (a) Capacity (left) and Coulombic efficiency (right) for cathodes based on 4-1-0, 4-1-1 and 4-1-2 cycled at 1 C rate. (b) First cycle galvanostatic charge–discharge profiles of 4-1-2-S nanocomposites at different C-rates from 0.1 C to 5 C. (c) Cyclic performance of 4-1-2-S nanocomposites at 2 C and 5 C rates. (d) A comparison of initial discharge capacities obtained from nanocomposites from HPCs and a commercial microporous activated carbon. (e) Cyclic performance at 2C and 5C rates, and (f) First cycle galvanostatic charge-discharge profiles at different C-rates from 0.1C to 5C, of commercial activated carbon-S nanocomposite.

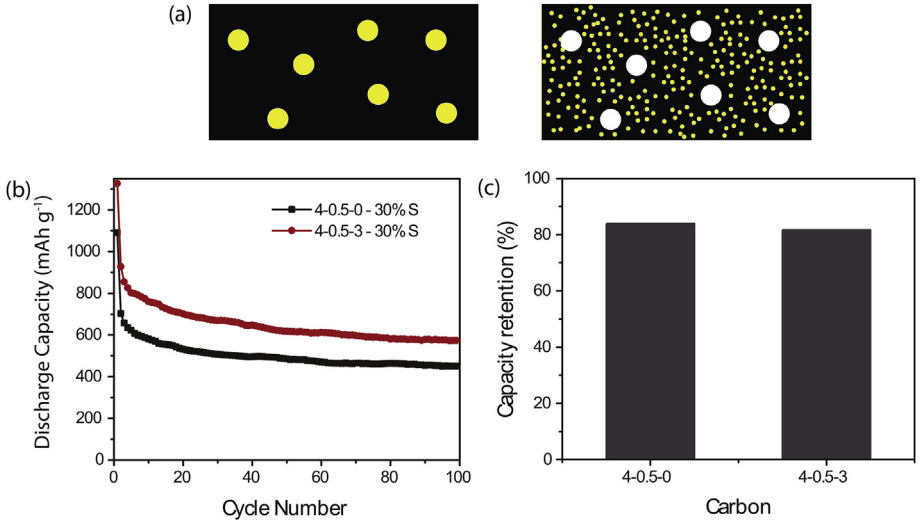

Fig. 4. (a) Schematic representation of distribution of sulfur in 30 wt. % S composites made with carbons 4-0.5-0 (left) and 4-0.5-3 (right) (b) Cyclic performance of the composites at 1 C rate (c) A bar graph comparing the capacity retention calculated from 10th–100th cycles for 30 wt. % S composites from 4-0.5-0 and 4-0.5-3 carbons.

phase by avoiding the formation of Li_2S, led to highly stable capacities [39,40].

4. Conclusions

A series of hierarchical porous carbons (HPCs) with exceptionally high surface areas and pore volumes, synthesized via a two-step process of hard templation followed by physical activation, were demonstrated to be excellent supports for sulfur for Li–S batteries. Physical activation of mesoporous carbons led to greatly increased surface areas and pore volumes due to the introduction of micro- and small mesopores while expanding the existing mesopores. The large surface areas caused sulfur to disperse well and the higher pore volume led to faster access to the dispersed sulfur by Li^+ ions, both favorable for better performance. Specific capacities at the 100th cycle @1 C increased from 555 mA h g^{-1} to 683 and 747 mA h g^{-1} after 1 h and 2 h of activation, respectively. Remarkably high capacities of 647 mA h g^{-1} and 503 mA h g^{-1} were still obtained after 200 cycles at high C-rates of 2 C and 5 C with relatively small electrode polarization, indicative of fast Li^+ ion kinetics. For comparison, a completely microporous carbon with high surface area under similar testing conditions delivered much lower capacity of 345 mA h g^{-1} at 100th cycle at 1 C. Moreover, a porosity-independent capacity fade is also systematically demonstrated in the presence of lithium nitrate electrolyte additive indicating effective elimination of capacity loss due to polysulfide shuttle. Facile and high throughput synthesis, tightly controlled and highly tunable porosity along with high power performance makes these HPCs a very promising platform for sulfur in lithium/sulfur batteries and good model system for other systematic studies.

Acknowledgments

This work is supported by the Energy Materials Center at Cornell (EMC^2) – an Energy Frontier Research Center funded by the U.S. Department of Energy, Office of Science, Office of Basic Energy Sciences (DE-SC0001086), King Abdullah University of Science and Technology (KAUST), KAUST baseline fund (KUS-C1-018-02). EPG acknowledges support from the NSF-PFI program (IIP-1114275). This work made use of the Cornell Center for Materials Research Shared Facilities supported through the NSF MRSEC program (DMR-1120296). We would like to thank Christos Tampaxis and Dr. Theodore Steriotis for their help with the porosity measurements, and, Mian Pan (Cornell University) and Tiffany Williams (Cornell University) for their help with Raman Spectroscopy of the carbons.

Appendix A. Supplementary data

Supplementary data related to this article can be found at http://dx.doi.org/10.1016/j.jpowsour.2015.07.068.

References

[1] B. Scrosati, J. Garche, J. Power Sources 195 (2010) 2419–2430.
[2] P.G. Bruce, S.A. Freunberger, L.J. Hardwick, J.M. Tarascon, Nat. Mater. 11 (2012) 19–29.
[3] B. Scrosati, J. Hassoun, Y.-K. Sun, Energy Environ. Sci. 4 (2011) 3287–3295.
[4] R.D. Rauh, F.S. Shuker, J.M. Marston, S.B. Brummer, J. Inorg. Nucl. Chem. 39 (1977) 1761–1766.
[5] S.S. Zhang, J. Power Sources 231 (2013) 153–162.
[6] Y.V. Mikhaylik, J.R. Akridge, J. Electrochem. Soc. 151 (2004) A1969.
[7] A. Manthiram, Y.Z. Fu, Y.S. Su, Acc. Chem. Res. 46 (2013) 1125–1134.
[8] M.K. Song, E.J. Cairns, Y.G. Zhang, Nanoscale 5 (2013) 2186–2204.
[9] X.L. Ji, K.T. Lee, L.F. Nazar, Nat. Mater. 8 (2009) 500–506.
[10] G. He, X.L. Ji, L. Nazar, Energy Environ. Sci. 4 (2011) 2878–2883.
[11] N. Jayaprakash, J. Shen, S.S. Moganty, A. Corona, L.A. Archer, Angew. Chem. Int. Ed. 50 (2011) 5904–5908.
[12] L.W. Ji, M.M. Rao, S. Aloni, L. Wang, E.J. Cairns, Y.G. Zhang, Energy Environ. Sci. 4 (2011) 5053–5059.
[13] J.L. Wang, J. Yang, J.Y. Xie, N.X. Xu, Y. Li, Electrochem. Commun. 4 (2002) 499–502.
[14] X.L. Li, Y.L. Cao, W. Qi, L.V. Saraf, J. Xiao, Z.M. Nie, J. Mietek, J.G. Zhang, B. Schwenzer, J. Liu, J. Mater. Chem. 21 (2011) 16603–16610.
[15] B. Ding, C.Z. Yuan, L.F. Shen, G.Y. Xu, P. Nie, X.G. Zhang, Chem. Eur. J. 19 (2013) 1013–1019.
[16] Y.S. Su, A. Manthiram, Nat. Commun. 3 (2012).
[17] R. Elazari, G. Salitra, A. Garsuch, A. Panchenko, D. Aurbach, Adv. Mater. 23 (2011) 5641–5644.
[18] J. Schuster, G. He, B. Mandlmeier, T. Yim, K.T. Lee, T. Bein, L.F. Nazar, Angew. Chem. Int. Ed. 51 (2012) 3591–3595.
[19] C. Lai, X.P. Gao, B. Zhang, T.Y. Yan, Z. Zhou, J. Phys. Chem. C 113 (2009) 4712–4716.
[20] H.B. Wu, S.Y. Wei, L. Zhang, R. Xu, H.H. Hng, X.W. Lou, Chem. Eur. J. 19 (2013) 10804–10808.
[21] B. Zhang, X. Qin, G.R. Li, X.P. Gao, Energy Environ. Sci. 3 (2010) 1531–1537.
[22] D.W. Wang, G.M. Zhou, F. Li, K.H. Wu, G.Q. Lu, H.M. Cheng, I.R. Gentle, Phys. Chem. Chem. Phys. 14 (2012) 8703–8710.
[23] C.D. Liang, N.J. Dudney, J.Y. Howe, Chem. Mater. 21 (2009) 4724–4730.
[24] Z. Li, L. Yuan, Z. Yi, Y. Sun, Y. Liu, Y. Jiang, Y. Shen, Y. Xin, Z. Zhang, Y. Huang, Adv. Energy Mater. 4 (2014).
[25] M.Q. Zhao, Q. Zhang, J.Q. Huang, G.L. Tian, J.Q. Nie, H.J. Peng, F. Wei, Nat. Commun. 5 (2014) 3410.
[26] G.Y. Xu, B. Ding, L.F. Shen, P. Nie, J.P. Han, X.G. Zhang, J. Mater. Chem. A 1 (2013) 4490–4496.
[27] S.C. Wei, H. Zhang, Y.Q. Huang, W.K. Wang, Y.Z. Xia, Z.B. Yu, Energy Environ. Sci. 4 (2011) 736–740.
[28] L.H. Yu, N. Brun, K. Sakaushi, J. Eckert, M.M. Titirici, Carbon 61 (2013) 245–253.
[29] S.R. Zhao, C.M. Li, W.K. Wang, H. Zhang, M.Y. Gao, X. Xiong, A.B. Wang, K.G. Yuan, Y.Q. Huang, F. Wang, J. Mater. Chem. A 1 (2013) 3334–3339.
[30] L. Estevez, R. Dua, N. Bhandari, A. Ramanujapuram, P. Wang, E.P. Giannelis, Energy Environ. Sci. 6 (2013) 1785–1790.
[31] Y.V. Mikhaylik, in, Google Patents, 2008.
[32] D. Aurbach, E. Pollak, R. Elazari, G. Salitra, C.S. Kelley, J. Affinito, J. Electrochem. Soc. 156 (2009) A694.
[33] G. Zheng, Y. Yang, J.J. Cha, S.S. Hong, Y. Cui, Nano Lett. 11 (2011) 4462–4467.
[34] S.S. Zhang, Electrochim. Acta 70 (2012) 344–348.
[35] S.S. Zhang, J.A. Read, J. Power Sources 200 (2012) 77–82.
[36] X. Liang, Z. Wen, Y. Liu, M. Wu, J. Jin, H. Zhang, X. Wu, J. Power Sources 196 (2011) 9839–9843.
[37] H. Sohn, M.L. Gordin, T. Xu, S. Chen, D. Lv, J. Song, A. Manivannan, D. Wang, ACS Appl, Mater. Interfaces 6 (2014) 7596–7606.
[38] S.S. Zhang, Electrochem. Commun. 31 (2013) 10–12.
[39] Y. Yang, G. Zheng, Y. Cui, Energy Environ. Sci. 6 (2013) 1552–1558.
[40] Y.-S. Su, Y. Fu, B. Guo, S. Dai, A. Manthiram, Chem. Eur. J. 19 (2013) 8621–8626.